World Journal of Environmental Biosciences
Available Online at: **www.environmentaljournals.org**

Volume 14, Issue 1: 1-9

https://doi.org/10.51847/gPX6I9ZEgK

ISSN 2277- 8047

Assessing the Effectiveness of Coprecipitation-Assisted ZnS/C Nanoclusters in the Photocatalytic Decomposition of 2,4-dichlorophenoxyacetic Acid Herbicide

Rajashekara Rakshitha[1], Haradhanahally Chandrashekara Sinchana[1], Nagaraju Pallavi[1*]

[1]Department of Environmental Science, School of Life Science, JSS Academy of Higher Education & Research, Mysuru-570015, India.

ABSTRACT

The elimination of organic contaminants from water is a critical issue in the modern day. Fortunately, photocatalytic technology has showcased its efficiency to remediate refractory persistent organic pollutants. A well-known herbicide 2,4-dichlorophenoxyacetic acid (2,4-D), is one such persistent organic pollutant in the majority of water sources. Herein, the photocatalytic activity of zinc sulfide/carbon (ZnS/C) was investigated in this work. Furthermore, The aforementioned nanocomposite was successfully created using the coprecipitation technique, and its constituent features were further examined using XRD, FTIR, FESEM, EDX, Zeta potential, and Tauc plot. The study aimed to optimize the following parameters: pH, pollutant concentration, contact time, and nanocomposite dose.
However, Maximum photocatalytic efficiency was 88.17 % at basic pH, for a pollutant concentration of 30 mg/L, with 0.8 mg/L of catalyst within 180 min of reaction. It is therefore the carbon doping with an active n-type semiconductor photocatalyst that boosted the photocatalytic action in the visible region Furthermore, for the next three cycles, ZnS/C had a fair degree of reusability. These experiments thus revealed that the ZnS/C nanocomposite that was created has great capabilities for 2,4-D remediation in an aqueous solution.

Keywords: *Photocatalysis, Nanocomposite, Coprecipitation, Persistent organic pollutant, 2,4- dichlorophenoxyacetic acid*

Corresponding author: Nagaraju Pallavi
e-mail ✉ anupallavi@jssuni.edu.in
Received: 24 November 2024
Accepted: 10 February 2025

INTRODUCTION

The increasing anthropogenic activities and the use of synthetic compounds in our lives have created a water crisis in the world (Belgiorno *et al*., 2007; Schwarzenbach *et al*., 2010; Kumar Reddy & Lee 2012; Prakruthi *et al*., 2021; Subramaniam *et al*., 2022). Specifically, the production and use of different chemicals, mainly for agricultural practices, pharmaceutics, and personal care are contributing to the widespread persistent organic pollutants (Sousa *et al*., 2018; Khasawneh & Palaniandy, 2021). The aquatic ecosystem is being accumulated as a result of the uncontrolled release of harmful pollutants into the environment, even at trace concentrations (Magro *et al*., 2020) and suggests human health effects. Numerous pests have evolved and changed agricultural systems, however, they are controlled by applying synthetic chemicals (Weber *et al*., 2018). Considering the increasing pesticide usage, this article attempts to address herbicides 2,4-D (de Castro Marcato *et al*., 2017). Technically, 2,4-D is a phenoxy compound, lethal to living things. 2,4-D has toxic effects on neurological tissue, including the brain and peripheral nerves (Natarajan *et al.,* 2021; Moja *et al*., 2024). This dangerous insecticide is rapidly absorbed by soil and water, contaminating natural resources. Therefore, to safeguard the environment, it is crucial to foster new materials that are environmentally friendly, economically viable, and employ effective methods for preventing and controlling organic pollution (Macur *et al*., 2007). In this direction, a sophisticated advanced oxidation process (AOP), which entails the *in-situ* creation of reactive oxidation radicals, efficient enough to break down and remove organic contaminants within environmental matrices, has been reported as a useful alternative technique (Bonora *et al*., 2020; Ghime & Ghosh, 2020; Paumo *et al*., 2021). Photocatalysis is one such AOP of heterogeneous nature driven by light energy, that has piqued research interest. It is superior for its low operating costs, nontoxicity, and effective contaminant reduction (Herrmann, 2005; Oturan & Aaron, 2014; Khoshnamvand *et al*., 2018; Ghime & Ghosh, 2020; Ashfaq *et al*., 2022).

Semiconductor photocatalysts are an excellent option as they are chemically inert, affordable, and have ease of preparation (Etacheri *et al.*, 2015; Gusain *et al*., 2019; Zhu & Zhou, 2019; Khan & Pathak, 2020; Roy *et al.*, 2020; Mohsin & Mohammed, 2021). Furthermore, it is thought to be essential to assess different photocatalysts for the breakdown of organic pollutants under LED light in order to progress toward sustainability (Liu *et al.*, 2013b; Oturan & Aaron, 2014; Puttaiah *et al*., 2019). ZnS is highly active in the UV region, however, could be easily modified to respond in the visible region. Popularly, using solid-state electronic moderators, such as carbon, enhances its efficiency (Lonkar *et al*., 2018). The following are the key benefits of utilizing carbonaceous mediators: visible light absorption is increased, photogenerated charges are transported and separated more effectively, increased surface area, inhibition of ZnS photo corrosion, and sufficient porous structure (Chen *et al*., 2017). To highlight a few important research findings, ZnS/C

nanostructures were employed by Ming *et al.* for the degradation of ciprofloxacin, methylene blue, and Rhodamine B (Cros *et al.*, 2015; Ming *et al.*, 2016). Here, under artificial sunlight (visible light), the as-produced hybrid materials demonstrated stronger photocatalytic activity than pure ZnS (> 380 nm), indicating a broad spectrum of photocatalytic destruction activity. Similarly, Bhavsar and the team reported ZnS/activated carbon for visible-light-driven Congo red decolourization. They came to the conclusion that the AC-ZnS nanocomposite's enhanced adsorption and decreased recombination rate of photoinduced charge pairs combined to produce greater photocatalytic efficiency (Mohammadi & Sabbaghi, 2014; Bhavsar *et al.*, 2021; Rajashekara *et al.*, 2024). Hence, In the current study, 2,4-D photodegradation with ZnS/C synthesized using a soft-chemical process under LED light is the main emphasis. Next, a thorough description of ZnS/C is provided, highlighting all of its fundamental physicochemical and photocatalytic properties. The study focused on process optimization by examining independent parameters such pH, catalyst dosage, contact time, and pollutant concentration.

MATERIALS AND METHODS

Chemicals and equipment

All chemicals and reagents utilized in this investigation were of analytical quality. Glucose, zinc acetate ($ZnC_4H_6O_4$), and sodium sulphide (Na_2S) were purchased from Sisco Research Laboratories Pvt. Ltd. India and were put to use without any additional cleansing. Laboratory-grade magnetic stirrer and a muffle furnace were used. Sodium hydroxide and hydrochloric acid solutions were used to properly alter the pH of the solutions.

Photocatalyst preparation

Carbon black was prepared by hydrolyzing 1 g of glucose in a microwave at 300° C (Schwenke *et al.*, 2015). To prepare pure ZnS, 10 ml of 1M zinc acetate was diluted with 75 ml of distilled water. Following this, 10 ml of 1M sodium sulphide was added dropwise after 1 hour of vigorous stirring. A white precipitate was produced, which was centrifuged to separate, then washed repeatedly with ethanol and double-distilled water. To obtain the powder sample, the precipitate was dried overnight at 50 °C under vacuum (Kripal *et al.*, 2010). Finally, to prepare ZnS/C, 0.3 g carbon black and 0.09 g Na_2S were refluxed in 100 ml distilled for 120 min. We used intermittent heating (1 min cycle) in between reactions to boost the reaction. The resultant black powder was then annealed for 45 min at 300° C. The resultant nanocomposites were created by combining varying amounts of carbon with a fixed amount of ZnS. Catalyst preparation is Schematic illustrated in **Figure 1**.

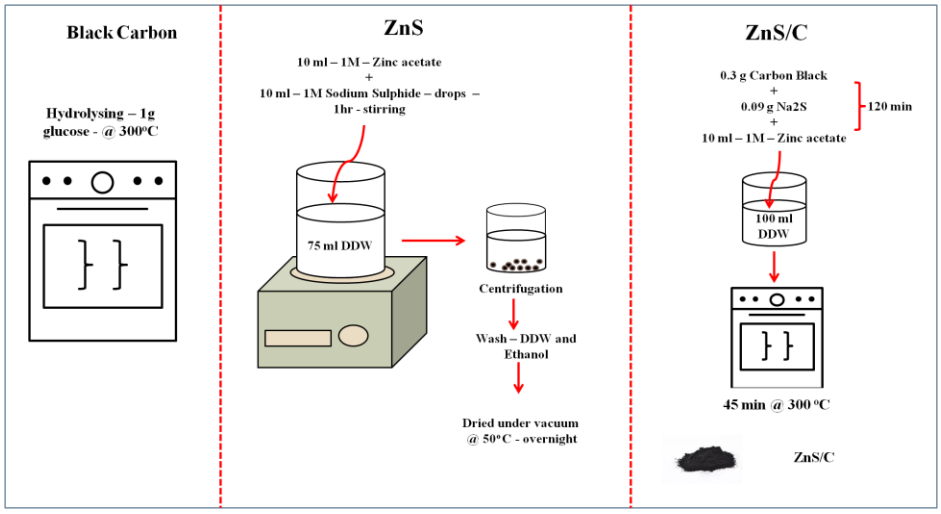

Figure 1. Schematic illustrations of the synthesis of ZnS/C nanocomposite

Characterization of ZnS/C

X-ray diffraction (XRD) patterns were recorded using the X-ray diffractometer (Microstar Proteum 8, Bruker). FT-IR was performed with a PerkinElmer RX-1 spectrophotometer using potassium bromide, to capture functional details. The field emission scanning electron microscope (FESEM) JSM-7100F (JEOL, Singapore) was used to study the morphological structure and elemental composition and particle size and Zeta potential measurements were recorded with the NANOTRAC WAVE II Q machine. The band energy was calculated using a UV-visible spectrophotometer (UV-1800, Shimadzu Corporation, Japan).

Photocatalytic performance assessment

The parameter optimization technique was employed for designing the experiments, which is an extensively used method for evaluating the effect of the interacting factors and for the optimization of the photocatalytic efficiency. The four main parameters were studied namely, the concentration of 2,4-D, quantity of ZnS/C, pH, and contact time to know their interacting effects as well as their effects on the photocatalytic degradation.

Initially, 75 mL of 2,4-D solution (known molarity) with a calculated amount of catalyst was stirred under the dark condition at room temperature for about 30 min to attain an adsorption/desorption equilibrium condition. Later the mixture was subjected to an LED of 18 W. Following light irradiation, little portions of the reaction solution (two to three

milliliters) were taken out, filtered through a 0.45 um syringe filter to extract the catalyst, and then measured at an absorbance of 285 nm using a UV-VIS Spectrophotometer. Eq. 1 was used to estimate the degradation efficiency based on the absorbance of the solution's initial and final concentrations (Giannakis *et al.*, 2017).

$$\text{Degradation } (\%) = \left(1 - \frac{C_t}{C_0}\right) * 100 = \left(1 - \frac{A_t}{A_0}\right) * 100 \quad (1)$$

where Ct and C0 represent the concentrations of 2,4-D at time 0 minutes and t minutes, respectively, and At and A0 are equivalent values of absorbance at a corresponding maximum wavelength for 2,4-D.

RESULTS AND DISCUSSION

Characterisation of ZnS/C nanocomposite

Crystallographic results were obtained by XRD at a scan rate of 2°/min using Cu-K radiation between 10° and 80°. **Figure 2a** depicts the XRD pattern for the as-produced ZnS/C nanocluster. The prominent peaks registered at 26.94°, 28.57°, 47.48°, 56.63°, 62.83°, and 68.04° are comparable to those of reference XRD pattern (JCPDS 80-0007) and previous reports (Gu *et al.*, 2007). The narrow and crisp diffraction pattern confirms that the synthesized ZnS/C composite has high crystallinity.

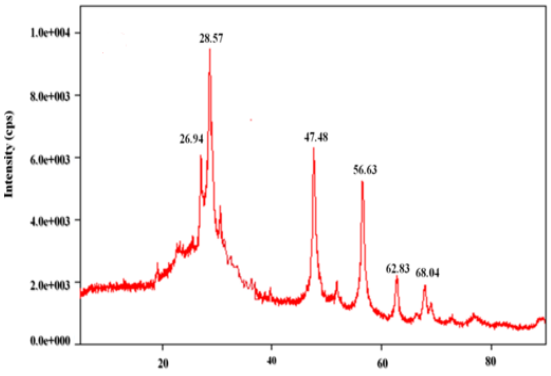

a)

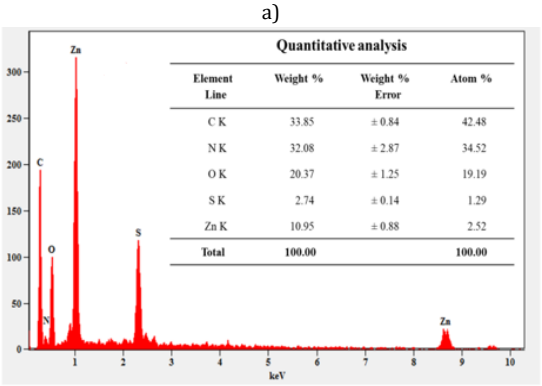

b)

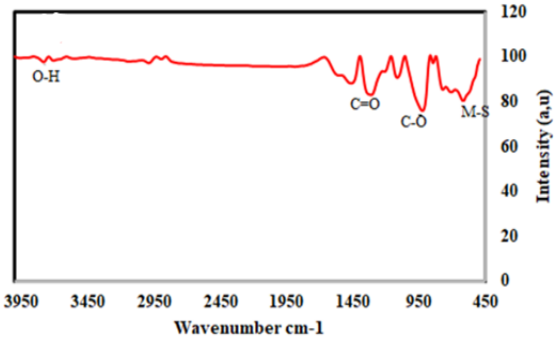

c)

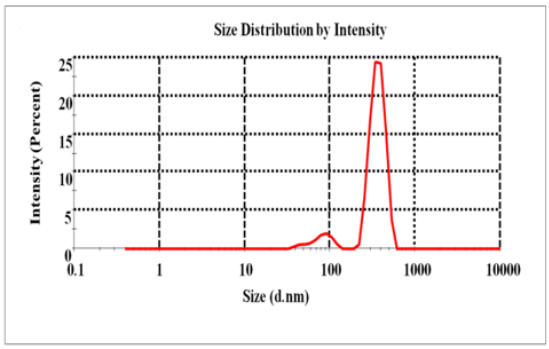

d)

Figure 2. a) XRD pattern of ZnS/C nanocomposite, b) Elemental composition by EDS and inset is the quantitative analysis of ZnS/C, c) FTIR spectra of ZnS/C nanocomposites and d) Size-dependent ZnS/C concentration intensity

By EDX analysis, the substance's elemental makeup was identified. **Figure 2b** illustrates the energy-dispersive spectrometry (EDS) results for the sample, which shows that C, Zn, and S are present in the results. One reason for the very small oxygen signal in the spectra is probably the inevitable surface adsorption of oxygen onto the samples from air exposure during sample processing. The sample comprises 2.52% Zn, 1.29% S, and 42.48% C, with 10.95% Zn, 2.74% S, and 33.85% C atomic percentage. The effective synthesis of ZnS/C is demonstrated by the EDX data. Similar findings can be seen in prior work (Gu *et al.*, 2007; Mehrizad & Gharbani, 2017).

Fourier transform infrared spectrophotometer is an analytical technique that shows the chemical properties of carbon-ZnS nanocomposite. **Figure 2c** displays the FT-IR spectral range of the synthesised sample ZnS nanoparticles. Peaks at 4000 and 500 cm^{-1} show the elongating group among metal and sulphur, as well as insufficient bands in both 3300 and 3500 cm-1 to O-H stretching vibration because of the absorption of moisture on nanoparticle surfaces. The band C-O, which is related to the presence of acetic acid in the primary substance, is assigned to a band between 937 and 1010 cm^{-1}. **Figure 5** shows the FT-IR spectra of pure carbon nanoparticles. The band was assigned the O-H stretching vibrations at 3441 cm-1, and C=O stretching mode was assigned to the bands between 1610 & 1713 cm^{-1}. Similarly, the resonance between the C-O and C=O modes is also related to a narrow spectrum at 1384 cm-1. Finally, **Figure 5** shows the Carbon-ZnS Nanocomposite's FT-IR spectrum. A poor band between 3000 and 3500 cm^{-1}, as

previously mentioned, are attributed to the O-H stretching mode, concentration peaks somewhere around 40-0 and 2000 cm^{-1}, and the elongating group both between metal and sulphur are exposed. The C-O band is assigned a frequency band at 937 as well as 990 cm^{-1} (Khosravi *et al*., 1995).

A Zeta potential was used to calculate the nanocomposite's surface potential. To estimate the surface charge and comprehend more about the physical stability of nanosuspensions, it is crucial to determine the zeta potential of nanostructures. DLS analysis was used to determine the catalysts' dynamic sizes as prepared. The ensuing **Figure 2d** displays the obtained outcomes. ZnS/C particles have an average dynamic size of 905.5 nm and are distributed throughout a narrow size range of 100-1000 nm.

The as-produced carbon-ZnS nanocomposite's morphology was examined under a microscope. **Figures 3a-3c** shows the FESEM micrographs, captured at X 20,000, X 30,000, and X 1, 00,000 magnifications, respectively. Carbon-ZnS nanocomposite has attained nanoclusters structures.

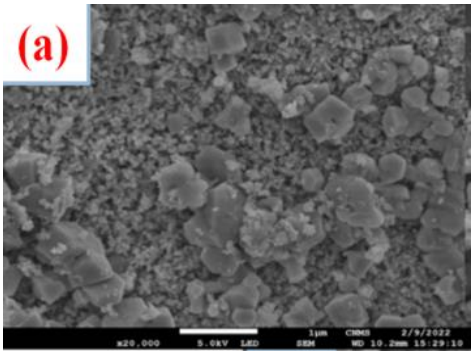

a)

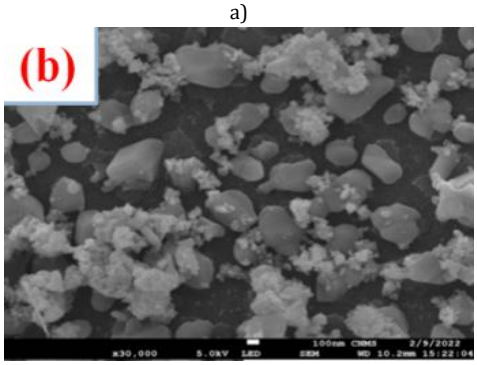

b)

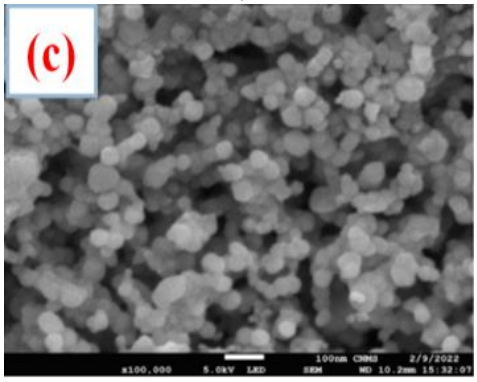

c)

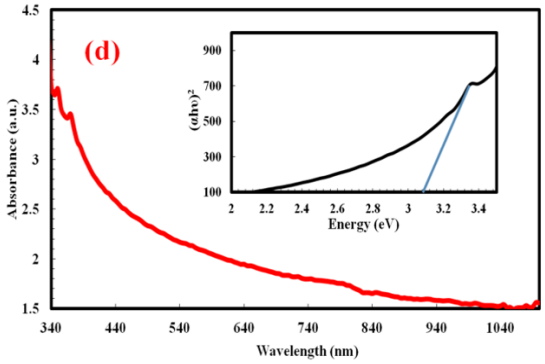

d)

Figure 3. a-c) FESEM images of ZnS/C at different magnification, and d) UV-Visible spectra and bandgap of ZnS/C

The UV-Vis spectra were used to show the light scattering capabilities and determine the bandgap of the semiconductor material as synthesized (Rakshitha *et al*., 2022). The UV-Vis spectra obtained in the wavelength range of 340-1040 nm are shown in **Figure 3d**. Previous studies (Neto *et al*., 2020) found that the optical bandgap (Eg) was 3.1 eV. Eq. 2 was utilized to calculate Eg, where h represents the Planck constant, is the frequency, and h is the incident photon energy (Rakshitha *et al*., 2022). The "h" vs. "h" curve for ZnS/C is shown in **Figure 3d**. This study showed that the ZnS/C nanocomposite's photocatalytic activity increased in the presence of visible light.

$$(\alpha h\upsilon) = A(h\upsilon - E\mathrm{g}) \qquad (2)$$

Parameter optimization for individual variables

To determine the ideal pollutant concentration, a series of experiments were performed with pollutant concentrations (2,4. D) ranging from 10, 20, 30, 40, 50, 60, 70, 80, 90, and 100mg/L, agitation rate 300rpm, contact period 90 min, pH 3.0, and catalyst dose of 0.2 mg/L were held constants. The maximum removal efficiency was obtained at 55.3% with 30 mg/L of 2,4 D concentration. **Figure 4a** illustrates a plot of pollutant degradation (2.4, D) vs removal percentage with constant independent variables. However, the rate of degradation for 30 mg/L 2,4 D was 55.3% demonstrating the effective mineralization of a lower analyte concentration. Whereas, from 40-100 mg/L of 2,4 D, the degradation decreased.

A series of tests were carried out to determine the ideal dose, changing the catalyst's concentration from 0.2, 0.4, 0.6, 0.8, and 1 mg/L with a constant pH of 3, a pollutant concentration of 30 mg/L, a rate of agitation of 300 ppm, and a contact time of 90 minutes. However, efficiency increased from 0.4 to 0.8 mg/L to >60%, while degradation decreased at 1 mg/L. The highest clearance rate recorded in this trial was 71.52% at a catalyst level of 0.8 mg/L, which was deemed ideal. A plot of Removal efficiency vs. catalyst dosage can be seen in **Figure 4b** (Georgekutty *et al*., 2008).

The investigation was conducted with varying pH ranges from 1 to 13 with constant catalysts dosage of 0.8mg/L, contact time of 90 minutes, pollutant concentration of 30mg/L, and 300 rpm agitating rate. As per the results obtained, a pH of 11 is the

ideal pH With maximum removal efficiency of 77.54 percent. However, it is noted that an alkaline condition is most suitable for 2,4 D removal. **Figure 4c** depicts a curve of 2.4, D removal efficiency against pH.

By varying the duration of the experiment the number of trials was conducted with constant pH 11, catalysts dosage of 0.8mg/L, pollutant concentration of 30mg/L, and 300 rpm agitating rate. Removal efficiency increases with increasing contact time. At 2 hours, virtual saturation was established, while equilibrium was reached after three hours, with a percentage removal of 81.26 per cent. There was no substantial reduction after 3 hours. **Figure 4d** depicts a graph of 2.4, D reduction from water as a function of contact time.

After obtaining the above results, the maximum removal efficiency was obtained with pH 11, catalyst dose 0.8 mg/L, pollutant concentration 30 mg/L, and contact time 180 min. To compute final optimization, and the highest percentage removal of 2,4 D the experiment was carried out for 3 trial runs and an average of 88.17 % removal was obtained by optimum condition. **Figure 5** depicts the results of 3 trail runs with optimum conditions with 2,4 D degradation.

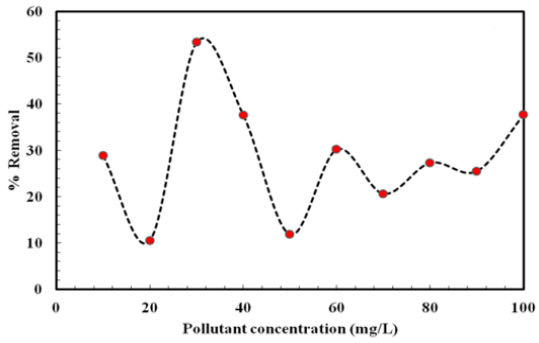

a)

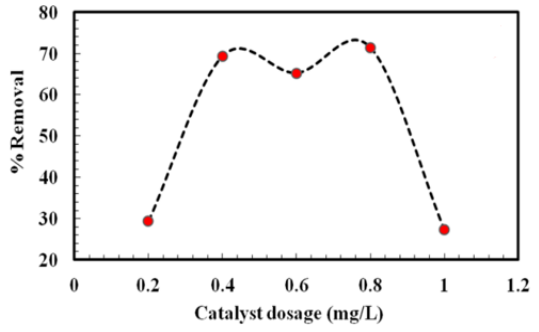

b)

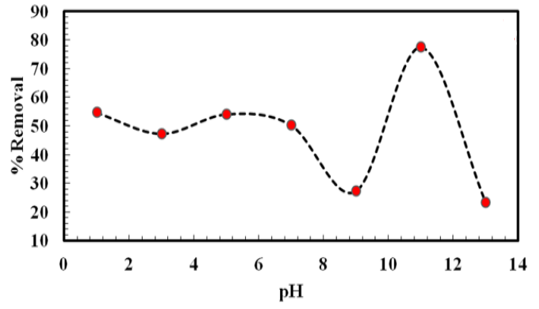

c)

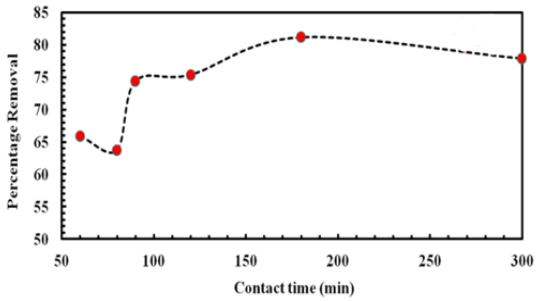

d)

Figure 4. a) Removal efficiency vs pollutant concentration plot with constant agitation rate 300rpm, contact period 90 min, pH 3.0, and catalyst dose of 0.2mg/L, b) Removal efficiency vs catalyst dosage plot with constant pH 3, pollutant concentration of 30 mg/L, agitating rate 30ppm, and contact time 90 minutes, c) Removal efficiency vs pH plot with constant catalysts dosage of 0.8mg/L, contact time of 90 minutes, pollutant concentration of 30mg/L, and 300 rpm agitating rate, and d) Removal efficiency vs contact time plot with pH 11, catalysts dosage of 0.8mg/L, pollutant concentration of 30mg/L, and 300 rpm agitating rate.

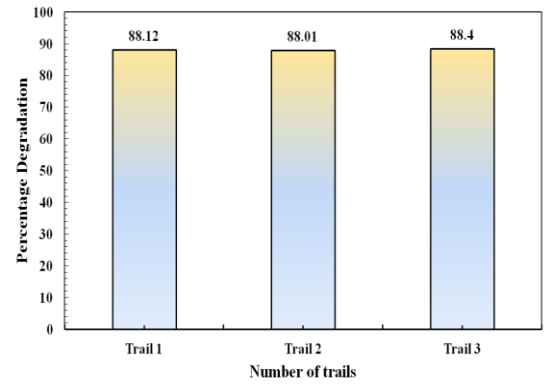

Figure 5. Percentage degradation of 2,4 D with the optimum condition at pH 11, catalyst dose 0.8 mg/L, pollutant concentration 30 mg/L, and contact time 180 min.

Photocatalytic mechanism

Electrons in the ZnS-carbon heterostructures are excited from their valence band (VB) state to the conduction band (CB) state by photo-irradiation, where they eventually combine to form electron-hole pairs. This transition leaves the VB with positively charged holes, which leads to the development of hydroxyl radicals. Similarly, the conduction band (CB) produces electrons that are reactive enough to reduce the molecular oxygen. Because of its potent oxidizing properties, the generated reactive radical species is highly effective at breaking down the pollutant 2,4 D. The reactive oxygen species hydroxyl radical and superoxide anion are created when these generated holes and electrons contact with the adsorbed oxygen and water molecules on the surface of the ZnS/C nanocomposite, respectively. Reactive oxygen species, or ROS, interact with the pollutant and break down its complex and dangerous chemical structure to produce non-toxic compounds like CO2 and H2O. During the 2,4 D degradation process, a number of OH radical-induced reactions, such as

hydroxylation, carboxylation, and ring cleavage, cause the breakdown of 2,4 D and produce CO2 and H2O along with innocuous degradation products (Rajesh *et al*., 2023). The photocatalytic mechanism is described below in Eqs. 3-8 (Rajesh *et al*., 2023; Ankita *et al*., 2024).

$$ZnS + h\nu \rightarrow ZnS + e^{-} + h^{+} \quad (3)$$

$$Carbon + h\nu \rightarrow Carbon + e^{-} + h^{+} \quad (4)$$

$$O_2 + e^{-} \rightarrow {}^{\bullet}O_2^{-} \quad (5)$$

$$h^{+} + H_2O \rightarrow {}^{\bullet}OH + H^{+} \quad (6)$$

$$h^{+} + OH^{-} \rightarrow {}^{\bullet}OH \quad (7)$$

$${}^{\bullet}O_2^{-} + {}^{\bullet}OH + pollutant \rightarrow CO_2 + H_2O + harmless\ degradation\ products \quad (8)$$

Effect of different sources of water

Various types of real-water samples were used in the current experiment to examine the photocatalytic effectiveness of the suggested ZnS/C nanocluster catalyst. For this study, residential wastewater, lake water, and tap water with a pollutant concentration of 30 mg/L were spiked. The effectiveness in each of these scenarios is depicted in **Figure 6a**. While tap water showed an efficiency decline of 11.7%, deionized water showed the highest percentage deterioration of 88.02%, which is optimised through RSM. However, the elimination of 2,4-D from lake water and domestic wastewater was 52.98% and 59.6%, respectivelyA significant decrease in efficiency can be attributed to the possible interaction of the various elements—organic and inorganic, metals and non-metals, etc.—found in lake water and domestic wastewater (Yashas *et al*., 2021; Rakshitha *et al.,* 2023).

The study noted the selectivity, chemical stability, and practical applicability of the photocatalyst and concluded that the 2,4 D mineralization capability of ZnS/C nanoclusters was acceptable and encouraging in all conditions.

Reusability of ZnS/C nanoclusters

One of the key elements in terms of long-term applicability is the ZnS/C nanoclusters' reusability or stability, which was tested using the cyclic mode. In this context, Three distinct cycles were used to test the reusability of ZnS/C nanoclusters at pH 11, 0.8 mg/L of catalyst dose, and 30 mg/L of pollutant concentration. For the next cycle, the catalyst was removed, cleaned, and oven-dried. The repeatability test results for three consecutive cycles are shown in **Figure 6b**. 2,4 D degrading efficiency has dropped from the first cycle by roughly 15.57 % by the end of the third. This could be the result of consecutive cycles diminishing the active surface sites of the catalyst. The results of the previous study are validated by ZnS/C nanoclusters for 2,4-D because of their excellent stability and reusability.

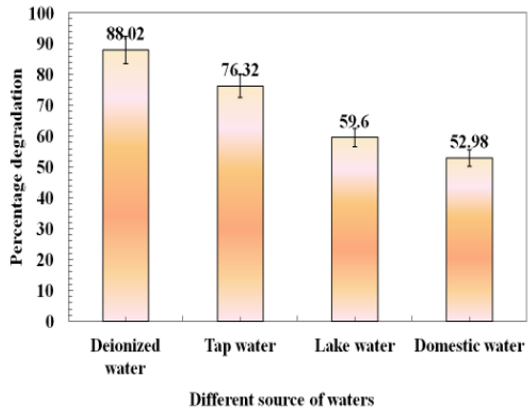

a)

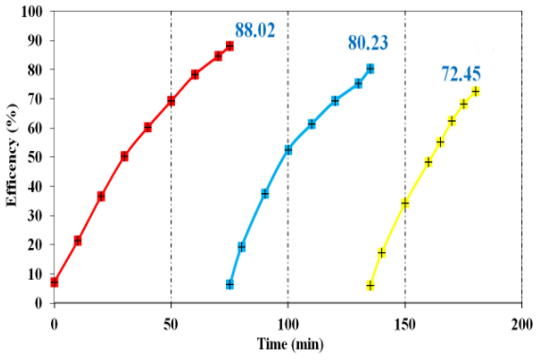

b)

Figure 6. a) Effect of 2,4-dichlorophenoxyacetic acid in different sources of water, and b) Reusability of ZnS/C nanoclusters.

Table 1. Comparison of ZnS/C nanocomposite with other similar work

Photocatalyst	Synthesis	Target	Efficiency (%)	Reference
C/ZnS/ZnO	hydrothermal	tetracycline (TC)	81%	(Zou *et al.*, 2019)
ZnS/CdS composites	solvothermal route with homogeneous precipitation process.	organic dyes (such as Methyl Orange, Pyronine B, Rhodamine B and Methylene Blue)	73% for Methylene Blue, 78% Rhodamine B, 68% Methyl Orange, 72% Pyronine B	(Liu *et al*., 2013a)
ZnS/C	Co-precipitation	2,4-D	88.02%	Present work

CONCLUSION

In this study, we adopted the co-precipitation approach to developing a ZnS/C nanocomposite at room temperature, which exhibited the remarkable photocatalytic degradation of 2,4-D with 88.17% degradation at 30mg/L pollutant concentration, 0.8 mg/L catalyst dosage under an alkaline environment at 180 minutes of contact time. Furthermore, the parameter optimization method has opted for the assessment of the 2.4.D photocatalytic degradation and to assess the

impact of four independent variables in the optimization process. A parameter optimization technique clarified the importance of the different parameters in the pollutant degradation process, including the concentration of pollutants, catalyst dosage, pH, and contact time. This study approved that the above synthesized ZnS/C nanocomposite was a promising photocatalyst for the degradation of 2.4, D. This finding demonstrated that organic contaminants decompose through neutral or base pH aqueous solutions was monitored to assess its photocatalytic function of the nanocomposites particles. As UV-IR radiation exposure time and nanocomposite content increased, the pollutant concentration rapidly decreased.

ACKNOWLEDGMENTS: None

CONFLICT OF INTEREST: None

FINANCIAL SUPPORT: None

ETHICS STATEMENT: None

REFERENCES

Ankita, B., Rakshitha, R., & Pallavi, N. (2024). Degradation of cefixime by photocatalysis via Ba-doped BiFeO3 nanomaterial using RSM analysis under LED light source. *Environmental Monitoring and Assessment*, *196*(7), 625. doi:10.1007/s10661-024-12781-1

Ashfaq, M., Talreja, N., Chauhan, D., Rodríguez, C. A., Mera, A. C., & Viswanathan, M. R. (2022). A facile synthesis of CuBi2O4 hierarchical dumbbell-shaped nanorod cluster: A promising photocatalyst for the degradation of caffeic acid. *Environmental Science and Pollution Research*, *29*(35), 53873-53883. doi:10.1007/s11356-022-19592-2

Belgiorno, V., Rizzo, L., Fatta, D., Della Rocca, C., Lofrano, G., Nikolaou, A., Naddeo, V., & Meric, S. (2007). Review on endocrine disrupting-emerging compounds in urban wastewater: Occurrence and removal by photocatalysis and ultrasonic irradiation for wastewater reuse. *Desalination*, *215*(1-3), 166-176. doi:10.1016/j.desal.2006.10.035

Bhavsar, K. S., Labhane, P. K., Murade, V. D., Dhake, R. B., & Sonawane, G. H. (2021). A photocatalyst: Zinc sulfides nanospheres immobilized on activated carbon for the abatement of aquatic organic pollutants. *Inorganic Chemistry Communications*, *133*, 108958. doi:10.1016/j.inoche.2021.108958

Bonora, R., Boaretti, C., Campea, L., Roso, M., Martucci, A., Modesti, M., & Lorenzetti, A. (2020). Combined AOPs for formaldehyde degradation using heterogeneous nanostructured catalysts. *Nanomaterials*, *10*(1), 148. doi:10.3390/nano10010148

Chen, F., Yang, Q., Wang, S., Yao, F., Sun, J., Wang, Y., Zhang, C., Li, X., Niu, C., Wang, D., et al. (2017). Graphene oxide and carbon nitride nanosheets co-modified silver chromate nanoparticles with enhanced visible-light photoactivity and anti-photocorrosion properties towards multiple refractory pollutants degradation. *Applied Catalysis B: Environmental*, *209*, 493-505. doi:10.1016/j.apcatb.2017.03.026

Cros, C. J., Terpeluk, A. L., Crain, N. E., Juenger, M. C., & Corsi, R. L. (2015). Influence of environmental factors on removal of oxides of nitrogen by a photocatalytic coating. *Journal of the Air & Waste Management Association*, *65*(8), 937-947. doi:10.1080/10962247.2015.1040524

de Castro Marcato, A. C., de Souza, C. P., & Fontanetti, C. S. (2017). Herbicide 2, 4-D: A review of toxicity on non-target organisms. *Water, Air, & Soil Pollution*, *228*, 1-12. doi:10.1007/s11270-017-3301-0

Etacheri, V., Di Valentin, C., Schneider, J., Bahnemann, D., & Pillai, S. C. (2015). Visible-light activation of TiO2 photocatalysts: Advances in theory and experiments. *Journal of Photochemistry and Photobiology C: Photochemistry Reviews*, *25*, 1-29. doi:10.1016/j.jphotochemrev.2015.08.003

Georgekutty, R., Seery, M. K., & Pillai, S. C. (2008). A highly efficient Ag-ZnO photocatalyst: Synthesis, properties, and mechanism. *The Journal of Physical Chemistry C*, *112*(35), 13563-13570. doi:10.1021/jp802729a

Ghime, D., & Ghosh, P. (2020). Advanced oxidation processes: A powerful treatment option for the removal of recalcitrant organic compounds. In *Advanced oxidation processes-Applications, trends, and prospects*. IntechOpen.

Giannakis, S., Rtimi, S., & Pulgarin, C. (2017). Light-assisted advanced oxidation processes for the elimination of chemical and microbiological pollution of wastewaters in developed and developing countries. *Molecules*, *22*(7), 1070. doi:10.3390/molecules22071070

Gu, F., Li, C., & Wang, S. (2007). Solution− chemical synthesis of carbon nanotube/ZnS nanoparticle core/shell heterostructures. *Inorganic Chemistry*, *46*(13), 5343-5348.

Gusain, R., Gupta, K., Joshi, P., & Khatri, O. P. (2019). Adsorptive removal and photocatalytic degradation of organic pollutants using metal oxides and their composites: A comprehensive review. *Advances in Colloid and Interface Science*, *272*, 102009. doi:10.1016/j.cis.2019.102009

Herrmann, J. M. (2005). Heterogeneous photocatalysis: State of the art and present applications. *Topics in Catalysis, 34*, 49-65. doi:10.1007/s11244-005-3788-2

Khan, S. H., & Pathak, B. (2020). Zinc oxide based photocatalytic degradation of persistent pesticides: A comprehensive review. *Environmental Nanotechnology, Monitoring & Management*, *13*, 100290. doi:10.1016/j.enmm.2020.100290

Khasawneh, O. F. S., & Palaniandy, P. (2021). Removal of organic pollutants from water by Fe2O3/TiO2 based photocatalytic degradation: A review. *Environmental Technology & Innovation*, *21*, 101230. doi:10.1016/j.eti.2020.101230

Khoshnamvand, N., Kord Mostafapour, F., Mohammadi, A., & Faraji, M. (2018). Response surface methodology (RSM) modeling to improve removal of ciprofloxacin from aqueous solutions in photocatalytic process using copper oxide nanoparticles (CuO/UV). *AMB Express*, *8*, 1-9. doi:10.1186/s13568-018-0579-2

Khosravi, A. A., Kundu, M., Kuruvilla, B. A., Shekhawat, G. S., Gupta, R. P., Sharma, A. K., Vyas, P. D., & Kulkarni, S. K. (1995). Manganese doped zinc sulphide nanoparticles by

aqueous method. *Applied Physics Letters*, *67*(17), 2506-2508. doi:10.1063/1.114440

Kripal, R., Gupta, A. K., Mishra, S. K., Srivastava, R. K., Pandey, A. C., & Prakash, S. G. (2010). Photoluminescence and photoconductivity of ZnS: Mn2+ nanoparticles synthesized via co-precipitation method. *Spectrochimica Acta Part A: Molecular and Biomolecular Spectroscopy*, *76*(5), 523-530. doi:10.1016/j.saa.2010.04.018

Kumar Reddy, D. H., & Lee, S. M. (2012). Water pollution and treatment technologies. *Journal of Environmental and Analytical Toxicology*, *2*, e103. doi:10.4172/2161-0525.1000e103

Liu, S., Li, H., & Yan, L. (2013a). Synthesis and photocatalytic activity of three-dimensional ZnS/CdS composites. *Materials Research Bulletin*, *48*(9), 3328-3334. doi:10.1016/j.materresbull.2013.05.055

Liu, S., Wang, X., Zhao, W., Wang, K., Sang, H., & He, Z. (2013b). Synthesis, characterization and enhanced photocatalytic performance of Ag2S-coupled ZnO/ZnS core/shell nanorods. *Journal of Alloys and Compounds*, *568*, 84-91. doi:10.1016/j.jallcom.2013.03.149

Lonkar, S. P., Pillai, V. V., & Alhassan, S. M. (2018). Facile and scalable production of heterostructured ZnS-ZnO/Graphene nano-photocatalysts for environmental remediation. *Scientific Reports*, *8*(1), 13401. doi:10.1038/s41598-018-31539-7

Macur, R. E., Wheeler, J. T., Burr, M. D., & Inskeep, W. P. (2007). Impacts of 2, 4-D application on soil microbial community structure and on populations associated with 2, 4-D degradation. *Microbiological Research*, *162*(1), 37-45. doi:10.1016/j.micres.2006.05.007

Magro, C., Mateus, E. P., Paz-Garcia, J. M., & Ribeiro, A. B. (2020). Emerging organic contaminants in wastewater: Understanding electrochemical reactors for triclosan and its by-products degradation. *Chemosphere*, *247*, 125758. doi:10.1016/j.chemosphere.2019.125758

Mehrizad, A., & Gharbani, P. (2017). Synthesis of ZnS decorated carbon fibers nanocomposite and its application in photocatalytic removal of Rhodamine 6G from aqueous solutions. *Progress in Color, Colorants and Coatings, 10*, 13-21.

Ming, F., Hong, J., Xu, X., & Wang, Z. (2016). Dandelion-like ZnS/carbon quantum dots hybrid materials with enhanced photocatalytic activity toward organic pollutants. *RSC Advances*, *6*(37), 31551-31558. doi:10.1039/C6RA02840C

Mohammadi, M., & Sabbaghi, S. J. E. N. (2014). Photo-catalytic degradation of 2, 4-DCP wastewater using MWCNT/TiO2 nano-composite activated by UV and solar light. *Environmental Nanotechnology, Monitoring & Management*, *1*, 24-29. doi:10.1016/j.enmm.2014.09.002

Mohsin, M. K., & Mohammed, A. A. (2021). Catalytic ozonation for removal of antibiotic oxy-tetracycline using zinc oxide nanoparticles. *Applied Water Science*, *11*(1), 9. doi:10.1007/s13201-020-01333-w

Moja, M. M., Mapossa, A. B., Chirwa, E. M. N., & Tichapondwa, S. (2024). Photocatalytic degradation of 2, 4-dichlorophenol using nanomaterials silver halide catalysts. *Environmental Science and Pollution Research*, *31*(8), 11857-11872. doi:10.1007/s11356-024-31921-1

Natarajan, T. S., Gopi, P. K., Natarajan, K., Bajaj, H. C., & Tayade, R. J. (2021). TiO2/graphene oxide nanocomposite with enhanced photocatalytic capacity for degradation of 2, 4-dichlorophenoxyacetic acid herbicide. *Water-Energy Nexus*, *4*, 103-112. doi:10.1016/j.wen.2021.07.001

Neto, N. A., Silva, J. M. P., Tranquilin, R. L., Longo, E., Bomio, M. R. D., & Motta, F. V. D. (2020). Stabilization of the γ-Ag2WO4 metastable pure phase by coprecipitation method using polyvinylpyrrolidone as surfactant: Photocatalytic property. *Ceramics International, 46*(10), 14864-14871. doi:10.1016/j.ceramint.2020.03.012

Oturan, M. A., & Aaron, J. J. (2014). Advanced oxidation processes in water/wastewater treatment: Principles and applications. A review. *Critical Reviews in Environmental Science and Technology*, *44*(23), 2577-2641. doi:10.1080/10643389.2013.829765

Paumo, H. K., Dalhatou, S., Katata-Seru, L. M., Kamdem, B. P., Tijani, J. O., Vishwanathan, V., Kane, A., & Bahadur, I. (2021). TiO2 assisted photocatalysts for degradation of emerging organic pollutants in water and wastewater. *Journal of Molecular Liquids*, *331*, 115458. doi:10.1016/j.molliq.2021.115458

Prakruthi, K., Ujwal, M. P., Yashas, S. R., Mahesh, B., Kumara Swamy, N., & Shivaraju, H. P. (2022). Recent advances in photocatalytic remediation of emerging organic pollutants using semiconducting metal oxides: An overview. *Environmental Science and Pollution Research*, *29*(4), 4930-4957.

Puttaiah, S. H., Menon, S., Ravindra, Y. S., Kumari, S., Revanna, H., & David, J. (2019) Preparation of supporting photocatalysts for water treatment using natural sunlight as an alternative driving energy. *Materials Today: Proceedings, 45*, 3936–3944. doi:10.1016/j.matpr.2020.08.020

Rajashekara, R., Raj, A. B. A., & Nagaraju, P. (2024). An RSM Modeling and Optimization: Utilizing Zn Nanoparticles for 2, 4-D Photocatalytic Degradation in Water. *Oriental Journal of Chemistry*, *40*(2), 535–546. doi:10.13005/ojc/400228

Rajesh, C., Rajashekara, R., & Nagaraju, P. (2023). Response Surface Methodology (RSM) modelling for the photocatalytic optimization study of benzophenone removal using CuWO4/NiO nanocomposite. *Journal of Environmental Health Science and Engineering*, *21*(1), 187-199. doi:10.1007/s40201-023-00852-3

Rakshitha, R., Gurupadayya, B., Devi, S. H. K., & Pallavi, N. (2022). Coprecipitation aided synthesis of bimetallic silver tungstate: A response surface simulation of sunlight-driven photocatalytic removal of 2, 4-dichlorophenol. *Environmental Science and Pollution Research*, *29*(39), 59433-59443. doi:10.1007/s11356-022-20062-y

Rakshitha, R., Rajesh, C., Gurupadayya, B., Devi, S. H. K., & Pallavi, N. (2023). A response surface modeling and optimization of photocatalytic degradation of 2, 4-dichlorophenol in water using hierarchical nano-assemblages of CuBi2O4 particles. *Environmental Science and Pollution Research*, *30*(30), 75655-75667. doi:10.1007/s11356-023-27774-9

Roy, N., Alex, S. A., Chandrasekaran, N., Mukherjee, A., & Kannabiran, K. (2021). A comprehensive update on

antibiotics as an emerging water pollutant and their removal using nano-structured photocatalysts. *Journal of Environmental Chemical Engineering*, *9*(2), 104796. doi:10.1016/j.jece.2020.104796

Schwarzenbach, R. P., Egli, T., Hofstetter, T. B., Von Gunten, U., & Wehrli, B. (2010). Global water pollution and human health. *Annual Review of Environment and Resources*, *35*(1), 109-136. doi:10.1146/annurev-environ-100809-125342

Schwenke, A. M., Hoeppener, S., & Schubert, U. S. (2015). Synthesis and modification of carbon nanomaterials utilizing microwave heating. *Advanced Materials*, *27*(28), 4113-4141. doi:10.1002/adma.201500472

Sousa, J. C., Ribeiro, A. R., Barbosa, M. O., Pereira, M. F. R., & Silva, A. M. (2018). A review on environmental monitoring of water organic pollutants identified by EU guidelines. *Journal of Hazardous Materials*, *344*, 146-162. doi:10.1016/j.jhazmat.2017.09.058

Subramaniam, M. N., Goh, P. S., Kanakaraju, D., Lim, J. W., Lau, W. J., & Ismail, A. F. (2022). Photocatalytic membranes: A new perspective for persistent organic pollutants removal. *Environmental Science and Pollution Research*, *29*(9), 12506-12530. doi:10.1007/s11356-021-14676-x

Weber, R., Herold, C., Hollert, H., Kamphues, J., Blepp, M., & Ballschmiter, K. (2018). Reviewing the relevance of dioxin and PCB sources for food from animal origin and the need for their inventory, control and management. *Environmental Sciences Europe*, *30*, 1-42. doi:10.1186/s12302-018-0166-9

Yashas, S. R., Shivaraju, H. P., McKay, G., Shahmoradi, B., Maleki, A., & Yetilmezsoy, K. (2021). Designing bi-functional silver delafossite bridged graphene oxide interfaces: Insights into synthesis, characterization, photocatalysis and bactericidal efficiency. *Chemical Engineering Journal*, *426*, 131729. doi:10.1016/j.cej.2021.131729

Zhu, D., & Zhou, Q. (2019). Action and mechanism of semiconductor photocatalysis on degradation of organic pollutants in water treatment: A review. *Environmental Nanotechnology, Monitoring & Management*, *12*, 100255. doi:10.1016/j.enmm.2019.100255

Zou, Z., Yang, X., Zhang, P., Zhang, Y., Yan, X., Zhou, R., Liu, D., Xu, L., & Gui, J. (2019). Trace carbon-hybridized ZnS/ZnO hollow nanospheres with multi-enhanced visible-light photocatalytic performance. *Journal of Alloys and Compounds*, *775*, 481-489. doi:10.1016/j.jallcom.2018.10.116